Significance of temperature increase in processing by high-pressure torsion

Edalati, Kaveh
Department of Materials Science and Engineering, Faculty of Engineering, Kyushu University |
WPI, International Institute for Carbon-Neutral Energy Research (I2CNER), Kyushu University

Miresmaeili, Reza
International Research Center for Hydrogen Energy, Kyushu University

Horita, Zenji
Department of Materials Science and Engineering, Faculty of Engineering, Kyushu University |
WPI, International Institute for Carbon-Neutral Energy Research (I2CNER), Kyushu University

Kanayama, Hiroshi
Department of Mechanical Engineering, Faculty of Engineering, Kyushu University

他

https://hdl.handle.net/2324/25615

Significance of temperature increase in processing by high-pressure torsion

Kaveh Edalati[a,b,]*, Reza Miresmaeili[c], Zenji Horita[a,b], Hiroshi Kanayama[d], Reinhard Pippan[e]

[a] Department of Materials Science and Engineering, Faculty of Engineering, Kyushu University, Fukuoka 819-0395, Japan

[b] WPI, International Institute for Carbon-Neutral Energy Research (I2CNER), Kyushu University, Fukuoka 819-0395, Japan

[c] International Research Center for Hydrogen Energy, Kyushu University, Fukuoka 819-0395, Japan

[d] Department of Mechanical Engineering, Faculty of Engineering, Kyushu University, Fukuoka 819-0395, Japan

[e] Christian Doppler Laboratory, Erich Schmid Institute of Materials Science, Austrian Academy of Sciences, Jahnstrasse 12, 8700 Leoben, Austria

Abstract

Experiments and finite element simulations were conducted to measure the temperature increase in processing disc samples by high-pressure torsion. Aluminum, copper, iron and molybdenum were selected as model materials. The temperature increases at the early stages of straining but saturates to steady-state levels at large strains. The increase of temperature is proportional to the hardness and rotation speed and is higher at higher imposed pressures and is somewhat higher at larger distances from the disc center.

Keywords: High-pressure torsion; Severe plastic deformation; Ultrafine-grained microstructure; Numerical computation; Temperature.

* Corresponding author at: Department of Materials Science and Engineering, Faculty of Engineering, Kyushu University, Fukuoka 819-0395, Japan.

Tel.: +81 92 802 2992; fax: +81 92 802 2992.

E-mail address: Kaveh.edalati@zaiko6.zaiko.kyushu-u.ac.jp (K. Edalati).

1. Introduction

Considerable interest has been developed over the last two decades in processing materials through the application of severe plastic deformation (SPD) [1,2]. Although several different SPD techniques are available, high-pressure torsion (HPT) appears to be especially effective in producing extremely small grain sizes and resultant high hardness values up to a steady sate [3–5]. Although HPT processing is generally used with thin disc samples with diameters of 10 mm [6–20] or ring samples with diameters of up to 40 mm [21,22], recent studies have developed the HPT process for use with disc samples with diameters of up to 40 mm [23], cylindrical bulk samples [24], ring samples with diameters of up to 100 mm [25] even including sheet and wire samples [26].

It is well documented that the microstructural evolution and deformation mechanisms are drastically influenced by processing temperature during plastic deformation [27]. A general question in processing by HPT concerns the magnitude of any temperature increase that occurs during the process. Although it is recognized that the temperature is raised during processing by HPT [28–31], there has been no systematic investigation to determine the temperature increase in the sample because of the difficulty in direct measurement under very high imposed pressures. The present study was thus initiated to measure the sample temperature in HPT processing. Four different pure metals were selected as model materials and the effect of processing time, rotation speed and imposed pressure on the temperature increase were investigated by means of experimental measurements and finite element (FEM) simulations.

2. Experimental materials and procedures

The principle of the HPT facility employed in this study is shown in Fig. 1. The facility consisted of upper and lower anvils made from SKD-11 martensitic tool steel having density, specific heat capacity and thermal conductivity values given in Table 1. Flat-bottom holes of 10 mm diameters and 0.25 mm depths were machined into the center of each anvil and the holes were subsequently roughened and nitrified to attain a surface roughness of ~30 μm and a microhardness of ~1000 Hv. These two anvils were fixed on two square-shaped steel plates and further assembled on two massive steel holders using four steel screws. The plates and the holders were separated from each other by using heat-insulation plates of 5 mm thickness.

The experiments were performed using the disc samples of high-purity Al (99.99%), Cu (99.99%), Fe (99.96%) and Mo (99.9%) with 10 mm diameters and 0.8 mm thickness. The details concerning the sample preparation before HPT and the evolution of microstructures and mechanical properties after HPT were reported elsewhere for Al [10,11,21,25], Cu [14,32], Fe [13,16,33] and Mo [20,34]. The thermal and physical properties of these metals, which were taken from Refs. [35,36], are given in Table 1. Each sample was placed on the shallow hole of the lower anvil and a pressure of P = 2 or 6 GPa was applied on the sample by raising the lower anvil up to a rigid contact with the upper anvil. The lower anvil was then rotated with respect to the upper anvil at room temperature (20 ◦C) with a rotation speed of either ω = 0.2, 0.5 or 1.0 rpm, and the rotation was terminated after N = 10 revolutions.

The temperature of the upper anvil at a radial distance of r = 3 mm from the rotation axis and a

height of z = 2.25 mm from the horizontal line were recorded every half second during processing using a K-type (chromel–alumel) thermocouple. The thermocouple was placed carefully in a hole fabricated in the upper anvil. Before each measurement, the calibration of thermocouple was checked at room temperature by comparing its measurements with the measurements of a precise thermometer. The temperatures of disc samples at z = 0 were further estimated using FEM simulations. Details about the FEM simulations are given below.

Table 1. Density, specific heat capacity and thermal conductivity values for Al, Cu, Fe, Mo and HPT anvils and plates.

	Density	Specific heat capacity	Thermal conductivity
	$(kg\ m^{-3})$	$(J\ Kg^{-1}\ K^{-1})$	$(W\ m^{-1}\ K^{-1})$
Al	2790	895	247
Cu	8960	385	398
Fe	7870	444	80
Mo	10200	247	142
Anvils and Plates	7700	460	40

2.1. Finite element simulations

The FEM simulations were employed using general purpose code MSC. Marc to solve a transient two-dimensional heat transfer within the cross-sectional plane along the longitudinal axis of the anvils and the plates. It is well known that heat is generated during plastic deformation because of plastic work. The amount of the plastic work per unit volume is given by [37]

$$U = \sigma\varepsilon \tag{1}$$

where σ is the flow stress and ε is the strain. Heat may also be generated due to pressure-induced effects (Q_p) like phase changes or the thermoelastic effect [37]. Therefore, the generated heat flux, ϕ, within a ring-shaped element of the HPT sample with mean radius of r, width of w and thickness of h is given by:

$$\phi = \frac{\beta\sigma\dot{\varepsilon}V + \dot{Q}_pV}{A} = \frac{(\beta\sigma\dot{\varepsilon} + \dot{Q}_P)(2\pi rwh)}{2\pi rw} \tag{2}$$

where β is the fraction of plastic work converted into heat, V is the volume of the element, $\dot{\varepsilon}$ is the strain rate, A is the horizontal area of the element and $\dot{Q}_P$ is the rate of heat generated per volume due to pressure induced effects. Compared to the heat generated due to the enormous strain Q_p is small and will be ignored. σ increases with the strain ε at the early stages of straining but saturates to steady-state levels at high strains [31–34]. β is smaller than one at the early stages of straining but reaches one at the steady state. ε is given by [37]

3

$$\varepsilon = \frac{2\pi rN}{h} = \frac{r\omega\, t}{h} \text{, and hence } \dot{\varepsilon} = \frac{r\omega}{h} \tag{3}$$

where ω is the rotation speed (angular velocity), t is the time and N the number of revolutions. Substituting Eq. (3) in Eq. (2), using $\beta = 1$ and ignoring the term of $\dot{Q}_P$ leads to:

$$\phi = \sigma.r\omega \tag{4}$$

Therefore, the heat flux is directly proportional to r and is independent of t. If a slippage takes place between the anvil and the sample, this will generate a frictional heat, Q_f [37]:

$$Q_f = F_f.l = \mu PAl \tag{5}$$

where F_f is the force of friction, l is the friction length and μ is the friction coefficient. Therefore, the generated heat flux, ϕ_s, due to slippage effect during HPT is given by:

$$\phi_s = \frac{\mu PAl}{At} = \frac{\mu P(2\pi rNs)}{t} = \mu sP.r\omega \tag{6}$$

where s is the fraction of slippage as described in an earlier work [38], and depends critically upon the material, pressure, rotation speed and the surface roughness of the anvils. Here, the fraction of slippage for Al, Cu, Fe and Mo are, respectively, 0, 0.12, 0.17 and 0.2 under a pressure of $P = 2$ GPa, and 0, 0, 0 and 0.25 under a pressure of $P = 6$ GPa [33,34,38]. When slippage occurs, ϕ due to plastic straining will decrease in proportion to $(1-s)$ [33]. P is usually larger than σ, however μ and s are smaller than 1, therefore the heat generated due to the occurrence of slippage will be compensated by the decrease of the plastic work. Hence, only the plastic work is taken into account in the FEM simulations in this study.

Although, the HPT method is essentially a thermo-mechanical process, the contribution of mechanical components to heat transfer simulations was considered using Eq. (4), and thus, the coupled thermal–mechanical simulation was reduced to a simple thermal simulation in this study. Here, the following assumptions were employed for the thermal simulations.

First, the geometry of the model was the same as the one shown in Fig. 1 and the thermal and physical properties of the sample, anvil and plates were those given in Table 1. Second, FEM mesh was established in MSC. Marc consisting of 16,249 nodes and 15,952 four-node isoparametric quadrilateral elements. Third, the plane at the mid-point of sample thickness and the contact area of two anvils, where a burr is formed, were considered as heat source. Fourth, the radius-dependent flux in the heat source during the HPT process was considered in the present FEM simulations by dividing the sample and the contact area of the two anvils into 12 heat sources having heat flux values proportional to the distance from the center. Fifth, the temperatures of screws were kept constant at room temperature and convection boundary conditions were applied on all air/metal boundaries with an air convection heat transfer coefficient of 50 W m^{-2} K^{-1}. Sixth, the heat flux was assumed zero for metal/insulator boundaries and the thermal and boundaries were considered as an average of the properties of the two neighboring materials.

The total generated heat and heat flux were primarily estimated from total plastic work and thereafter were determined carefully by fitting the temperature data of numerical computations to

the ones of experimental observations at z = 2.25 mm, r = 3 mm and N = 10. The temperature distributions in the sample, anvils and plates were further obtained using simulation results.
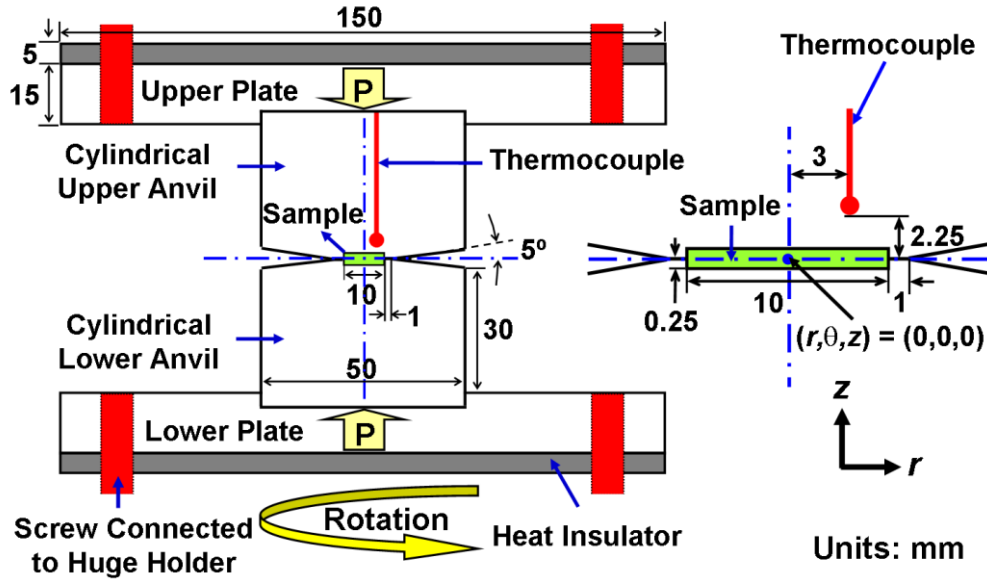

Fig. 1. Schematic illustration of HPT facility.

3. Results and discussion

The temperature values, measured experimentally at (z = 2.25 mm, r = 3 mm) and determined numerically by FEM simulations at (z = 2.25 mm, r = 3 mm) and at (z = 0, r = 5 mm), are plotted in Fig. 2 against time for (a) Al, (b) Cu and (c) Fe after N = 10 at ω = 0.2, 0.5, 1.0 rpm and P = 2 GPa. Fig. 3 shows the temperature values, measured experimentally at (z = 2.25 mm, r = 3 mm) and determined numerically by FEM simulations at (z = 2.25 mm, r = 3 mm) and at (z = 0, r = 5 mm) for the four model metals after N = 10 at ω = 1.0 rpm and P = 6 GPa. The simulation results in Fig. 3 were extended to N = 120 or t = 7200s. Inspection of Figs. 2 and 3 leads to several conclusions. First, the trends of the experimental measurements are well consistent with the results of FEM simulations at (z = 2.25, r = 3 mm), indicating that the assumptions applied for the FEM simulations are acceptable. It should be noted that only the applied assumptions in this study, which are based on the physical facts, could lead to an acceptable agreement between the trend of measured and simulated temperatures in this study. Second, the temperature increases significantly at the early stages of processing but levels off and reaches steady state where the temperature remains unchanged with processing time due to a balance between the rate of heat generation in the sample and the rate of cooling in the anvils. Third, the temperature increases with increasing speed of rotation in the torsional straining. Fourth, the temperature is dependent upon the material used for HPT processing and it is the lowest for Al but increases for the harder materials. Fifth, the temperature decreases with decreasing applied pressure. Close inspection of Fig. 3 reveals that a temperature peak appears after loading the pressure but before torsional straining by HPT. This peak must be primarily because of the thermoelastic effect in the anvils and partly because of the

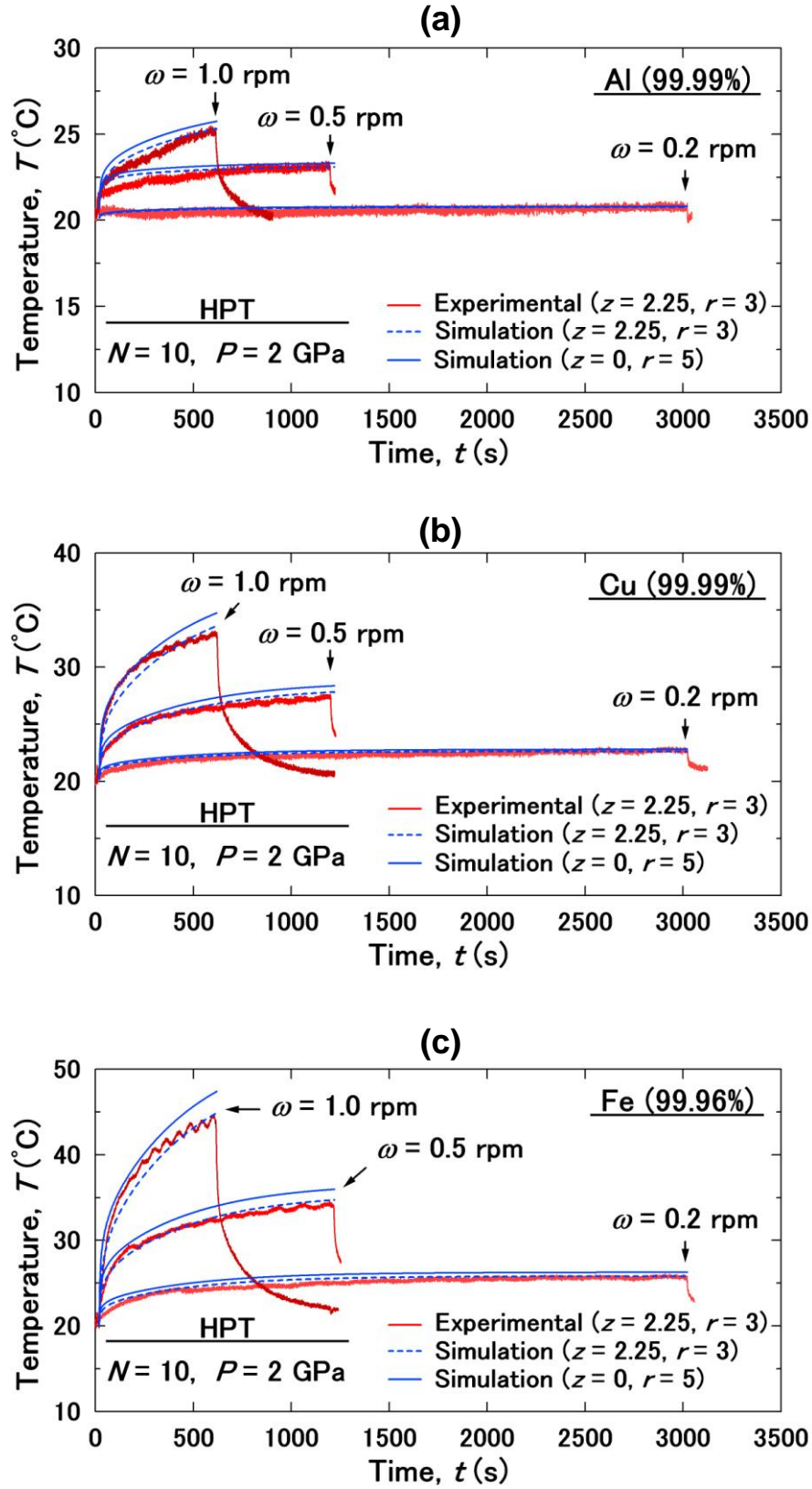initial compression of the samples.

(a)

(b)

(c)

Fig. 2. Temperatures at (z = 2.25 mm, r = 3 mm) and at (z = 0, r = 5 mm) versus time obtained by experimental measurements and FEM simulations for (a) Al, (b) Cu and (c) Fe after N = 10 at ω = 0.2, 0.5 and 1.0 rpm and P = 2 GPa.
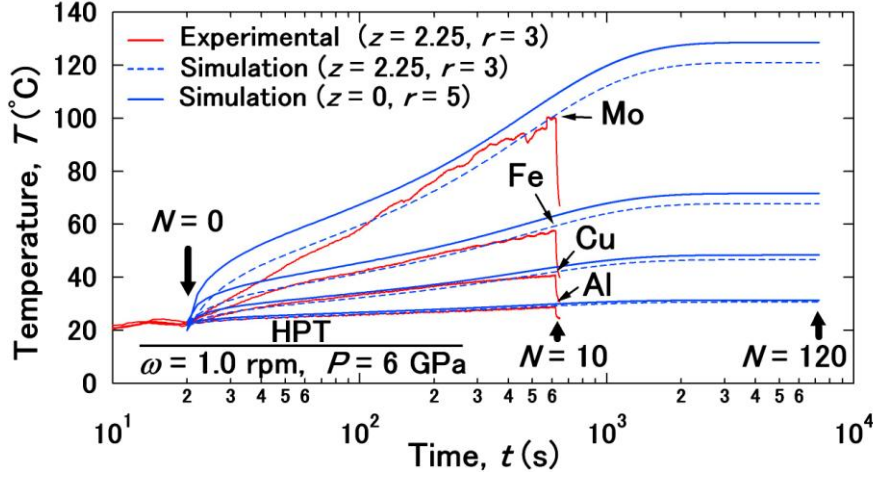
Fig. 3. Temperatures at (z = 2.25 mm, r = 3 mm) and at (z = 0, r = 5 mm) versus time obtained by experimental measurements and FEM simulations for four model metals after N = 10 or 120 at ω = 1.0 rpm and P = 6 GPa.

Since the heat flux at the steady state is proportional to the temperature increase within the sample ($\phi \propto \Delta T$), Eq. (3) suggests that ΔT is approximately proportional to ω and σ as far as the temperatures are evaluated at the steady state and at a given r. Since σ and the hardness at the steady state (HV_S) are proportional, the temperature values after N = 10, as indicated by the arrows in Figs. 2 and 3, are now plotted in Fig. 4 in the form of ΔT (after the subtraction of room temperature) against (a) HV_S and (b) $HV_S\omega$. The values of HV_S are 32 Hv for Al [25], 132 Hv for Cu [32], 308 Hv for Fe [33] and 680 Hv for Mo [34]. It is apparent from Fig. 4 that ΔT increases in proportion to HV_S and $HV_S\omega$ for given r, N and P, and this is consistent with Eq. (4). Furthermore, these plots suggest that the temperature increase becomes more significant at higher pressures. For instance, the extent of temperature increase at P = 6 GPa are ~1.5 times of those at P = 2 GPa for Al, Cu and Fe after N = 10 at ω = 1.0 rpm. The strong pressure effect is induced by the contribution of friction from the burr regime of the sample (see Eq. (4)) because this neglected contribution is proportional to P [39]. The uncertainties in the estimation of this part are the reasons for the experimental calibration of the simulation.

The FEM simulation results after processing at ω = 1.0 rpm and P = 6 GPa are shown in Figs. 5–7, where Fig. 5 shows the contours of temperature distribution in the anvils and plates including the total generated heat for four model metals after N = 10, Fig. 6 shows the contours of temperature distribution in the sample and anvils for Fe after revolutions from N = (1/8)-120, and Fig. 7 plots the sample temperature variation with the distance from the disc center for Fe after N = 10. Four important points are obtained from Figs. 5 and 6. First, the degree of any heat generation in the sample during processing by HPT is higher for harder materials: 16 kJ for Al, 41 kJ for Cu, 73 kJ for Fe and 155 kJ for Mo. Second, the degrees of heat generation obtained using simulations are well consistent with the amounts of plastic work, indicating that the assumptions applied for the FEM simulations in this study are valid. Using Eq. (1), considering V = 63 mm^3 for HPT discs, σ = 3 Hv, ε = 278 (average imposed strain after N = 10 revolutions) leads to plastic work values as 7 kJ

for Al, 28 kJ for Cu, 64 kJ for Fe and 142 kJ for Mo. The difference between these values and the values obtained by the simulations are 9–13 kJ. These differences which are independent of the material must be due to the contribution of frictional work from the burr regime of the sample. Third, the generated heats after $N = 10$ are as much as 10–20% of the heat needed to melt a disc sample. The heat needed to melt 1 mm^3 of material are 2.87 kJ for Al, 5.94 kJ for Cu, 11.04 kJ for Fe and 12.05 kJ for Mo [35]. Forth, the temperature is a minimum at the disc center and increases as the distance from the disc center increases. Fifth, the maximum temperature is reached in the contact area between the upper and lower anvils where a thin layer of sample presents between the two anvils. This thin layer, which is beneficial to eliminate direct contact and friction between the two anvils, experiences a frictional work as well as a giant torsional straining during processing by HPT due to its small thickness.
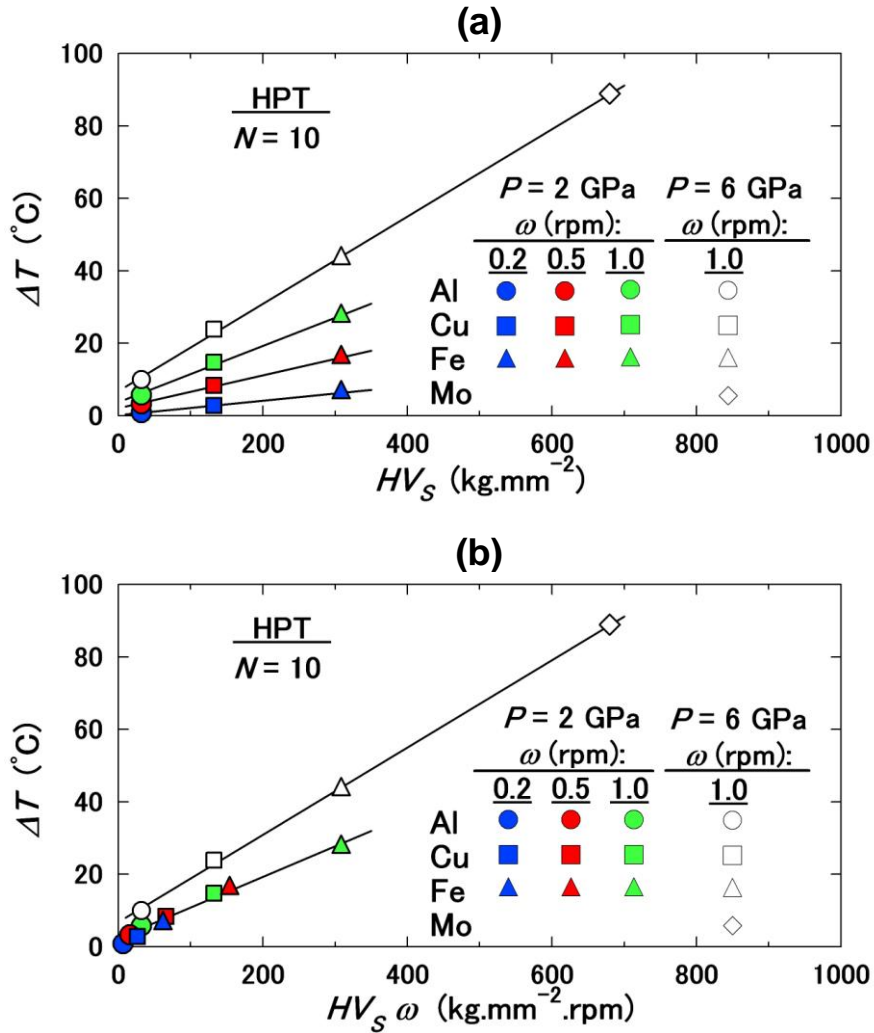

Fig. 4. Plots of ΔT against (a) HV_S and (b) $HV_S\omega$ for four model metals processed at $N = 10$, $\omega = 0.2$, 0.5 and 1.0 rpm, and $P = 2$ GPa. ΔT, temperature increases in sample obtained by FEM simulations; HV_S, steady-state hardness taken from Refs. [25,32–34]; ω, rotation speed.
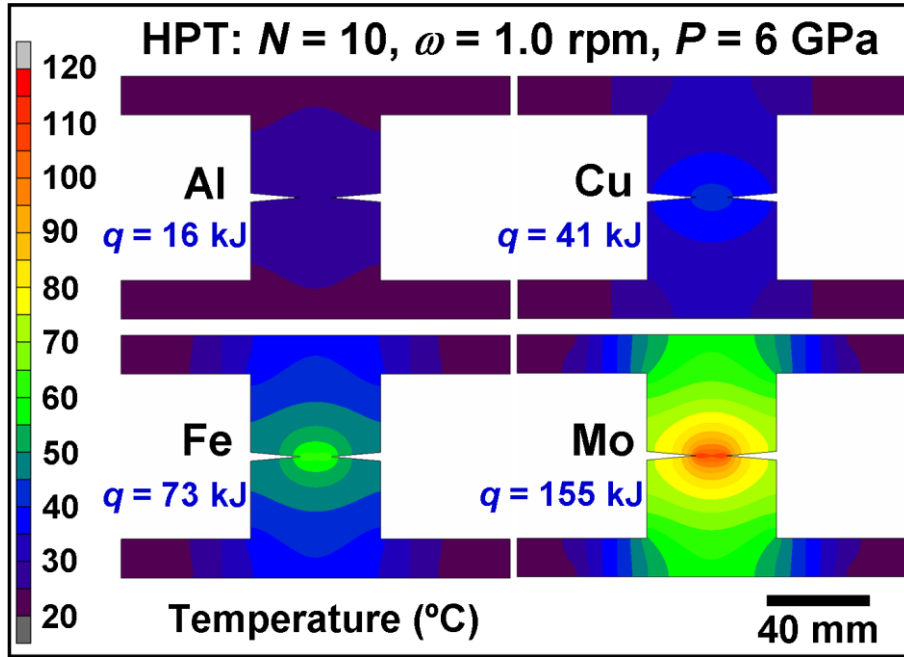
Fig. 5. FEM simulation results: contours of temperature distribution in anvils and plates including total generated heat for four model metals after $N = 10$ at $\omega = 1.0$ rpm and $P = 6$ GPa.
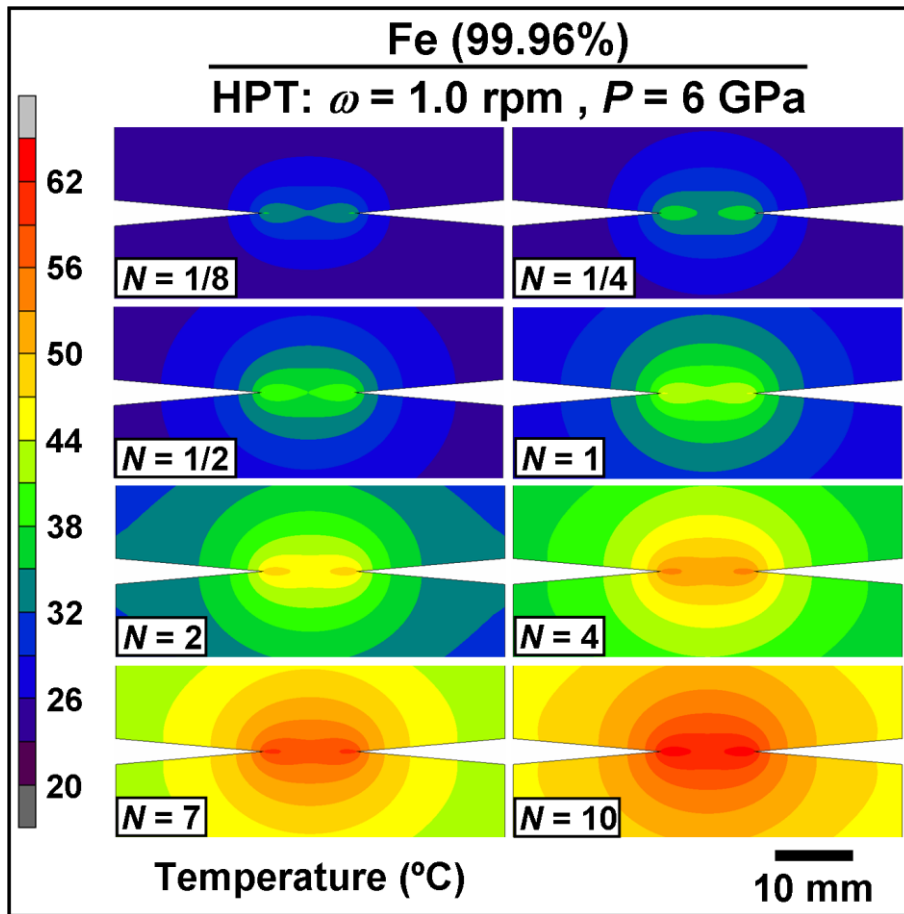

Fig. 6. FEM simulation results: contours of temperature distribution in sample and anvils for Fe after $N = 1/8–120$ at $\omega = 1.0$ rpm and $P = 6$ GPa.
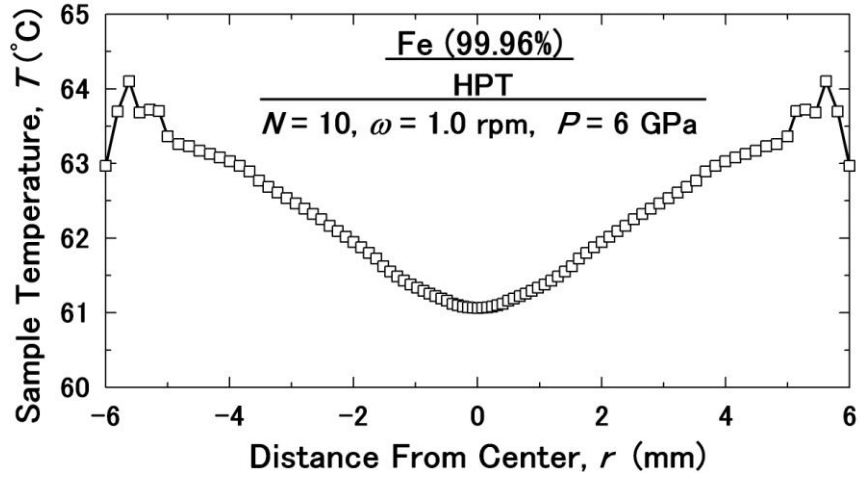
Fig. 7. FEM simulation results: sample temperature versus distance from disc center for Fe after N = 10 at ω = 1.0 rpm and P = 6 GPa.

The present investigation confirms that despite giant plastic deformation during processing by HPT, the degrees of temperature increase are not significant when compared to the melting temperatures of the selected model metals. It should be noted that the present results were recorded using small disc samples and a set of massive anvils and plates connected to huge holders which all act as effectual heat sinks. It is reasonable to anticipate that the temperature increase may be larger if the anvils are smaller, or surrounded by heat insulators, or connected to smaller plates and holders. Moreover, if either the sample size increases, or the contact area of two anvils becomes larger, or the slippage become more significant, or the two anvils rub together directly at the contact area, the temperature increase will become more significant.

4. Conclusions

In summary, the current study provides new findings on the temperature increase during processing by HPT. The results show the temperature increase depends upon the material and it is higher for harder materials. For all materials, the temperature increase becomes more significant with increasing the processing time, rotation speed, imposed pressure and distance from the disc center. To avoid a significant temperature increase during HPT the reduction of rotation speed is most efficient.

References

[1] R.Z. Valiev, Y. Estrin, Z. Horita, T.G. Langdon, M.J. Zehetbauer, Y.T. Zhu, JOM 58 (4) (2006) 33–39.

[2] R.Z. Valiev, R.K. Islamgaliev, I.V. Alexandrov, Prog. Mater. Sci. 45 (2000) 103–189.

[3] A.P. Zhilyaev, T.G. Langdon, Prog. Mater. Sci. 53 (2008) 893–979.

[4] F. Wetscher, R. Pippan, Philos. Mag. 86 (2006) 5867–5883.

[5] A. Vorhauer, R. Pippan, Scripta Mater. 51 (2004) 921–925.

[6] A.P. Zhilyaev, S. Lee, G.V. Nurislamova, R.Z. Valiev, T.G. Langdon, Scripta Mater. 44 (2001) 2753–2758.

[7] B.J. Bonarski, E. Schafler, B. Mingler, W. Skrotzki, B. Mikulowski, M.J. Zehetbauer, J. Mater. Sci. 43 (2008) 753–7518.

[8] V.V. Stolyarov, Y.T. Zhu, T.C. Lowe, R.K. Islamgaliev, R.Z. Valiev, Mater. Sci. Eng. A 282 (2000) 78–85.

[9] M.T. Perez-Prado, A.A. Gimazov, O.A. Ruano, M.E. Kassnerc, A.P. Zhilyaev, Scripta Mater. 58 (2008) 219–222.

[10] M. Kawasaki, B. Ahn, T.G. Langdon, J. Mater. Sci. 45 (2010) 4583–4593.

[11] M. Kawasaki, R.B. Figueiredo, T.G. Langdon, Acta Mater. 59 (2011) 308–316.

[12] Y. Todaka, M. Umemoto, A. Yamazaki, J. Sasaki, K. Tsuchiya, Mater. Trans. 49 (2008) 47–53.

[13] Y. Todaka, Y. Miki, M. Umemoto, C. Wang, K. Tsuchiya:, Mater. Sci. Forum 584–586 (2008) 597–602.

[14] G. Khatibi, J. Horky, B. Weiss, M. Zehetbauer, Int. J. Fatigue 32 (2010) 269–278.

[15] X.Z. Liao, Y.H. Zhao, S.G. Srinivasan, Y.T. Zhu, R.Z. Valiev, D.V. Gunderov, Appl. Phys. Lett. 84 (2004) 592–594.

[16] R.Z. Valiev, Y.U.V. Ivanisenko, E.F. Rauch, B. Baudelet, Acta. Mater. 44 (1996) 4705–4712.

[17] N. Boucharat, R. Hebert, H. Rosner, R.Z. Valiev, G. Wilde, Scripta Mater. 53 (2005) 823–828.

[18] A.R. Yavari, W.J. Botta, C.A.D. Rodrigues, C. Cardoso, R.Z. Valiev, Scripta Mater. 46 (2002) 711–716.

[19] J. Sort, D.C. Ile, A.P. Zhilyaev, A. Concustell, T. Czeppe, M. Stoica, S. Surinach, J. Eckert, M.D. Baro, Scripta Mater. 50 (2004) 1221–1225.

[20] Y.R. Kolobov, B. Kieback, K.V. Ivanov, T. Weissgaerber, N.V. Girsova, Y.I. Pochivalov, G.P. Grabovetskaya, M.B. Ivanov, V.U. Kazyhanov, I.V. Alexandrov, Int. J. Refract. Met. Hard Mater. 21 (2003) 69–73.

[21] Y. Harai, Y. Ito, Z. Horita, Scripta Mater. 58 (2008) 469–472.

[22] Y. Harai, K. Edalati, Z. Horita, T.G. Langdon, Acta Mater. 57 (2009) 1147–1153.

[23] R. Pippan, S. Scheriau, A. Taylor, M. Hafok, A. Hohenwarter, A. Bachmaier, Annu. Rev. Mater. Res. 40 (2010) 319–343.

[24] G. Sakai, K. Nakamura, Z. Horita, T.G. Langdon, Mater. Sci. Eng. A 406 (2005) 268–273.

[25] K. Edalati, Z. Horita, Mater. Trans. 50 (2009) 92–95.

[26] K. Edalati, Z. Horita, J. Mater. Sci. 45 (2010) 4578–4582.

[27] H.J. Frost, M.F. Ashby, Deformation-Mechanism Maps: The Plasticity and Creep of Metals and Ceramics, Pergamon Press, Oxford, 1982.

[28] A.P. Zhilyaev, J.M. Garcia-Infanta, F. Carreno, T.G. Langdon, O.A. Ruano, Scripta Mater. 57 (2007) 763–765.

[29] Y. Todaka, M. Umemoto, A. Yamazaki, J. Sasaki, K. Tsuchiya, Mater. Trans. 49 (2008) 7–14.

[30] S. Hober, Z. Kovacs, A. Revesz, J. Alloys Compd. 495 (2010) 352–355.

[31] K. Edalati, E. Matsubara, Z. Horita, Metall. Mater. Trans. A 40 (2009) 2079–2086.

[32] K. Edalati, T. Fujioka, Z. Horita, Mater. Sci. Eng. A 497 (2008) 168–173.

[33] K. Edalati, T. Fujioka, Z. Horita, Mater. Trans. 50 (2009) 44–50.

[34] S.W. Lee, K. Edalati, Z. Horita, Mater. Trans. 51 (2010) 1072–1079.

[35] A. Buch, Short Handbook of Metal Elements Properties and Elastic Properties of Pure Metals, third ed., Krzysztof Biesaga, Warasaw, 2005.

[36] Metals Handbook, Properties and Selection of Nonferrous Alloys and Special-Purpose Materials, vol. 2, ASM International, Metals Park, Ohio, 1990.

[37] G.E. Dieter, Mechanical Metallurgy, third ed., McGraw-Hill, New York, NY, 1976.

[38] K. Edalati, Z. Horita, T.G. Langdon, Scripta Mater. 60 (2009) 9–12.